Hindawi
Journal of Nanomaterials
Volume 2020, Article ID 6749150, 20 pages
https://doi.org/10.1155/2020/6749150

Research Article

An Effective Method for Hybrid CNT/GNP Dispersion and Its Effects on the Mechanical, Microstructural, Thermal, and Electrical Properties of Multifunctional Cementitious Composites

Mohammadmahdi Abedi,[1,2] **Raul Fangueiro**,[3,4] **and Antonio Gomes Correia**[1,2]

[1]*Department of Civil Engineering, University of Minho, Campus de Azurém, 4800-058 Guimarães, Portugal*
[2]*Institute for Sustainability and Innovation in Structural Engineering, University of Minho, Guimarães, Portugal*
[3]*Department of Mechanical Engineering, University of Minho, Campus de Azurém, 4800-058 Guimarães, Portugal*
[4]*Center for Textile Science and Technology, University of Minho, Campus de Azurém, 4800-058 Guimarães, Portugal*

Correspondence should be addressed to Raul Fangueiro; rfangueiro@dem.uminho.pt

Received 2 March 2020; Revised 18 May 2020; Accepted 23 June 2020; Published 17 July 2020

Academic Editor: Hiromasa Nishikiori

This paper reports a study undertaken to achieve a compatible and affordable technique for the high-quality dispersion of carbon nanotubes (CNTs) and graphene nanoplatelets (GNPs) in an aqueous suspension to be used in multifunctional cementitious composites. In this research work, two noncovalent surfactants with different dispersion mechanisms (Pluronic F-127 (nonionic) and sodium dodecylbenzene sulfonate (SDBS) (ionic)) were used. We evaluated the influences of various factors on the dispersion quality, such as the surfactant concentration, sonication time, and temperature using UV-visible spectroscopy, optical microscopic image analysis, zeta potentials, and particle size measurement. The effect of tributyl phosphate (TBP) used as an antifoam agent was also evaluated. The optimum suspensions of each surfactant were used to produce cementitious composites, and their mechanical, microstructural, electrical, and thermal behaviors were assessed and analyzed. The best dispersed CNT+GNP aqueous suspensions using Pluronic and SDBS were obtained for concentrations of 10% and 5%, respectively, with 3 hours of sonication, at 40°C, with TBP used for both surfactants. The results also demonstrate that cementitious composites reinforced with CNT+GNP/Pluronic showed better mechanical performance and microstructural characteristics due to the higher quality of the dispersion and the increasing hydration rate. Composites prepared with an SDBS suspension demonstrated lower electrical and thermal conductivities compared to those of the Pluronic suspension due to changes in the intrinsic properties of CNTs and GNPs by the SDBS dispersion mechanism.

1. Introduction

Various types of multifunctional cementitious composites employing carbon fillers have attracted widespread attention due to their potential applications, including monitoring, thermal management, and transportation [1–4]. Among carbon fillers, carbon nanotubes (CNTs) and graphene nanoplatelets (GNPs) are the most widely used fillers to improve the mechanical, microstructural, electrical, and thermal behavior of composites due to their unique properties, including their small size, low density, high stiffness, high strength, and excellent electronic and thermal conductivity [5]. CNTs and GNPs can act as a nucleation agent and raise the hydration rate in cementitious composites [6]. Graphene is a 2D monolayer of sp^2-hybridized carbon atoms arranged in a hexagonal packed lattice structure, and CNTs are 1D nanoscale tubes with an empty inner cavity that consists of single or multiple graphite atomic layers that are curved back on themselves [5, 7].

The high aspect ratio and large specific surface area of GNPs lead to a high contact area between composites and nanofillers and cause a maximized transferred stress and phonon transference from the matrix to the nanofillers. Hence, GNP-reinforced composites can be expected to

exhibit better mechanical, thermal, and electrical behavior even in comparison to CNTs [8]. However, in many cases, the potential applications of GNPs and CNTs are limited due to their high aspect ratio and large specific surface, which leads to large van der Waals forces and strong π -π interactions originating entanglement and agglomeration [9]. This is particularly important in multifunctional cementitious composites that normally use high concentrations of nanofillers to obtain higher electrical or thermal efficiency [10] (causing agglomerate formation and reducing their mechanical and microstructural performance [11]), since the physical properties are of significant importance in multifunctional cementitious composites [12].

Recently, several studies have been conducted to measure the CNT+GNP hybrid effects on multifunctional polymeric composites. The results show an improvement in the mechanical, microstructural, electrical, and thermal performance in comparison to their individual usage. Hence, the synergic effects of CNT+GNP combinations can decrease the required concentration of carbon nanomaterials (CNMs) by reducing the percolation threshold and subsequently significantly alleviating concerns regarding the costs and formation of porosities [8, 9, 13, 14]. Although no study has been found on the development of multifunctional cementitious composites of CNT+GNP combinations, we expect similar assumptions for this type of matrix. The combination of 1D (CNT) and 2D (GNP) nanoparticles with a high aspect ratio can increase the electron quantum tunneling effect as well as the percolation mechanism. CNT+GNP combinations can increase the hydration rate more than each would individually, due to the larger specific surface area that acts as a nucleation agent [6, 15]. They can also fill a wider range of micro- and nanopores, which leads to denser microstructures and bridges the hydration products of cement. However, a compatible and effective technique is required for the dispersion of CNT+GNP combinations in cementitious matrices, due to their agglomerate potential.

Therefore, our present study proposes a compatible and affordable method for the high-quality dispersion of CNT +GNP in multifunctional cementitious composites. Various chemical, biological, and physical techniques, such as high shear mixing, ultrasonication, ball milling, plasma, calendaring and irradiation methods, and noncovalent and covalent functionalization, have been extensively studied to modify and improve GNP and CNT dispersion in various matrices [16–25]. Although they often have an adverse effect on nanoparticles and/or composite features, preparing dispersed CNT and GNP suspensions through the noncovalent functionalization method does not alter the inherent optical, electrical, or mechanical properties of these nanoparticles. CNTs and GNPs are commonly dispersed along this route using different surfactants, aromatic small molecules, polymers, the endohedral method, and biomacromolecules [10, 24–42].

Currently, Pluronic F-127 (PF-127) is receiving increased attention among the different surfactants due to its lower toxicity and higher biocompatibility compared to other surfactants [43–47]. Pluronic F-127 (PF-127) is a nonionic triblock copolymer consisting of a core hydrophobic chain of polyoxypropylene (PPO) flanked by two polyoxyethylene (PEO) hydrophilic chains. As PF-127 has an amphiphilic structure, it has been asserted to be an efficient surfactant for the dispersion of CNTs and GNPs [44, 48]. Pluronic F-127 has great solubility in water at room temperature, allowing the preparation of CNT suspensions at a high surfactant concentration ratio. Due to the long PEO chain presence, Pluronic F-127 was found to be compatible with cementitious composites and demonstrated good mechanical behavior and dry bulk density possibly due to the high fluidity of mortar and dispersion of cement particles [49, 50].

Pluronic F-127 surfactants also exhibited a stronger ability to disperse MWCNTs in basic aqueous or extremely acidic media compared to ionic surfactants [30, 51]. MWCNTs were also effectively dispersed in ethoxy-modified composites of Pluronic F-127 and a silicone surfactant (trisiloxane). Sodium dodecylbenzene sulfonate (SDBS) is also a noncovalent surfactant that is commonly used to disperse carbon nanoparticles as it shows low interference with the performance of nanoparticles [49]. The effective dispersion of SWCNTs at high concentrations (up to 2 wt%) has been obtained recently, using the ionic surfactant SDBS through long-term ultrasonication treatment (24 hours) [52]. To disperse different types of CNTs and GNPs, the efficiency of SDBS has been reported as even higher than dodecyl-/tetradecyl-/cetyl-trimethylammonium bromide (DTAB/TTAB/CTAB), gum arabic (GA), nonylphenoxypoly(ethyleneoxy)ethanol (NP-10), cetylpyridinium chloride (CPyCl), and sodium dodecyl sulfate (SDS) [53–56].

Hence, the effects of Pluronic F-127 and SDBS on the stability of prepared suspensions of 1% CNT+GNP (0.5 wt% CNT and 0.5 wt% GNP) were evaluated for various concentrations, ultrasonication times, and temperatures and for the presence of tributyl phosphate (TBP, as an antifoam agent) in order to propose a compatible and affordable method for high-quality dispersions of CNT+GNP in multifunctional cementitious composites. We evaluated the effects of the optimally dispersed CNT+GNP suspensions on the microstructure and mechanical, thermal, and electrical behaviors of the cementitious composites, to ensure the efficiency of the technique and the absence of adverse effects.

2. Materials and Methods

2.1. Raw Materials. Carbon nanotubes and graphene nanoplatelets were purchased from CNPLUS Company (USA). Table 1 summarizes the characteristics of the GNPs and CNTs as provided by the manufacturer [57, 58]. Raman spectroscopy (Figure 1) was conducted on CNTs and GNPs using a HORIBA LabRAM HR Evolution confocal Raman microscope spectrometer through laser excitation with a wavelength of 532 nm.

We characterized the morphologies of GNPs and CNTs in different modes using a scanning electron microscope (SEM) (Figure 2). Pluronic F-127 and SDBS were used as surfactants in order to facilitate the CNT and GNP dispersion, and tributyl phosphate (TBP) was also used as an antifoam agent with 1/2 of the surfactant weight ratio. The surfactants and antifoam were purchased from Sigma-

Table 1: GNP and CNT characteristics.

GNP										
Surface area (m^2 g^{-1})	Density (g/cm^3)	Carbon content (%)	Tensile modulus (Gpa)	pH value (30°C)	Tensile strength (GPa)	Layers	Dimension		Form	Part number
120–150	0.6	>99.5	1000	7–7.65	5	<20	Thickness 4–20 nm	Diameter 5–10 μm	Gray powder	TGN201
MWCNT										
Surface area (m^2 g^{-1})	Density (g/cm^3)	Color	Outside diameter (nm)	Length (μm)	Ash (wt%)		Carbon content (%)		Part number	
350	0.27	Black	<8	30–10	<1.5		>98		GCM327	

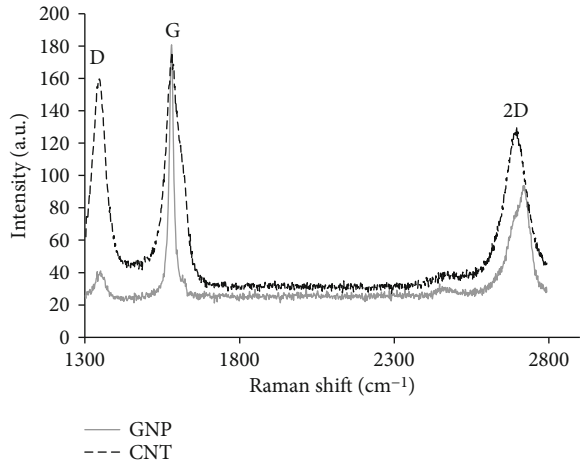

Figure 1: Carbon nanotube (CNT) and graphene nanoplatelet (GNP) Raman analysis.

Aldrich (Portugal) [59]. Their chemical structures are presented in Figure 3 [59, 60].

Ordinary Portland cement type I and CEN Standard sand (EN 196-1 and ISO 679:2009) from the SNL company were used to prepare cementitious composites (mortar). The particle size distribution of the sand and chemical composition of the ordinary Portland cement (OPC) are shown in Tables 2 and 3 [61].

2.2. CNT+GNP Dispersion. We dispersed 1% of CNT+GNP (wt of water) in aqueous solution by 5%, 10%, and 15% of each surfactant. The surfactant was first added to the water and mixed for 1 hour using a magnetic stirring mixer with a speed of 800 rpm/min. CNT+GNP was then added to the solution and stirred for one additional hour. The samples were then placed in a sonicator bath (Crest Ultrasonicator, CP 230T) for 1, 2, and 3 h, at 45 kHz frequency and 80 W power, at different temperatures.

A digital temperature regulator (NESLAB RTE-111 MP) was used to adjust the temperature during the ultrasonication process with a circulation system through a radiator and sensors. The TBP was completely dissolved in water before the addition of the surfactant.

2.3. Cementitious Composite Fabrication. Plain and CNT +GNP-reinforced specimens were prepared by mixing optimized CNT+GNP aqueous suspensions with ordinary Portland cement and standardized sand, using a laboratory mixer, following the EN 196-1:1994 standard. In all samples, a cement-to-water ratio of 0.5 was used. At first, the required amount of cement (450 g) was poured in the mixer's stainless steel bowl in order to prepare the mortar mixtures. Then, the prepared CNT+GNP suspension with 125 g of water was added to the cement and the required amount of sand (1350 g), and the remaining 100 g of water was poured into the mixing machine's hopper. The mixer was then run for 1.5 min, with a stainless steel blade rotational speed of 140 m/min, followed by a 30 s timeout, and then run at 285 m/min for another 2.5 min. The mixture was placed into 160 mm × 40mm × 40mm and 40mm × 40mm × 40mm (for the capillarity test) prismatic molds and placed on a jolting machine for 1 min for vibrating compaction. The molds were placed in a humid atmosphere (90%) for 24 h, and then, the samples were demolded and kept under water for 28 days. Two copper meshes of 40mm × 50 mm were embedded in the cementitious composite as electrodes, at 5 cm from the middle of the specimen, to measure the electrical behavior.

2.4. Characterization of CNT+GNP Aqueous Suspensions. Different techniques were used for characterizing various parameters of the prepared CNT+GNP suspensions.

2.4.1. UV-Visible Spectroscopy. Due to the additional absorption caused by 1D van Hove singularities, the dispersed carbon nanotubes and graphene nanoplatelets in aqueous suspensions are active in the region of UV-Vis [28, 62, 63]. Hence, we used UV-Vis spectroscopy (Shimadzu, UV 2401 PC) to evaluate the dispersed CNT+GNP concentrations in different aqueous suspensions. However, bundled carbon nanomaterials (CNMs) are extremely active in the wavelength region between 200 and 1200 nm due to the quenching of photoluminescence, which results in a weak and wide signal [49]. A solution with the same concentration of the surfactant agent was used as the blank sample to eliminate the peaks provided by the surfactant.

2.4.2. Zeta Potential and Particle Size Measurement. The zeta potential and bundle size of the carbon nanomaterials (CNM) were determined using the Zetasizer Malvern Nano ZS system in aqueous suspensions. The dynamic light scattering (DLS) technique has been used for measuring the

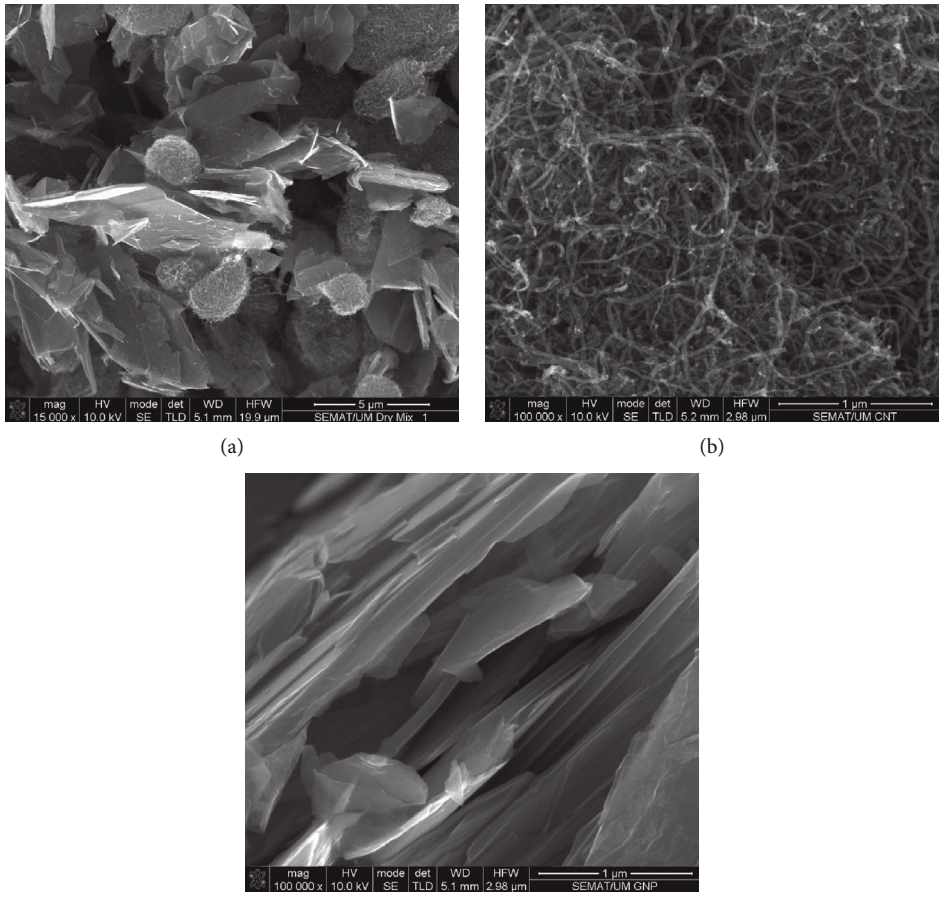

(a) (b) (c)

Figure 2: Morphology of (a) the CNT and GNP dry mix, (b) CNTs, and (c) GNPs.

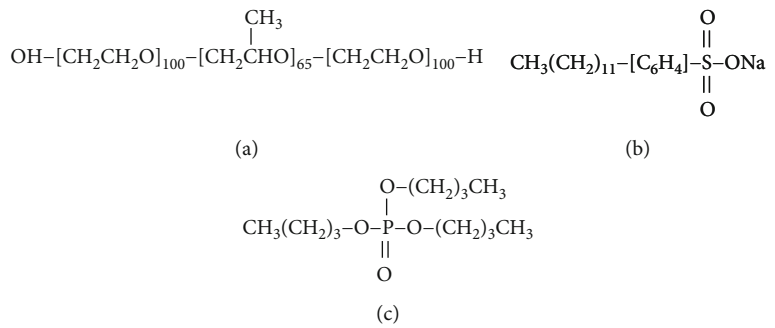

(a) (b) (c)

Figure 3: The chemical structures of (a) Pluronic F-127, (b) sodium dodecylbenzene sulfonate (SDBS), and (c) tributyl phosphate (TBP).

Table 2: Particle size distribution of the sand [61].

Mesh size (mm)	0.08	0.16	0.5	1	1.6	2
Cumulative retained (%)	99 ± 1	87 ± 5	67 ± 5	33 ± 5	7 ± 5	0

bundle size of CNM in aqueous suspensions; however, this technique is more accurate for perfectly spherical particles [49, 64, 65]. The results of CNM particle size determinations may highly be affected by their orientation toward the laser source and the combined morphology due to their high aspect ratio. Therefore, the analysis of the CNM particle size results was performed while considering these factors. The zeta potential (ζ) was determined using Equation (1) and the Smoluchowski approximation from electrophoretic mobility (μ).

$$\mu = \frac{\zeta \epsilon_m V}{4\pi\eta D}, \tag{1}$$

Table 3: Chemical composition and properties of ordinary Portland cement.

SiO_2	Al_2O_3	Fe_2O_3	MgO	CaO	Na_2O	TiO_2	K_2O	MnO	P_2O_5	SO_3	LOI	Fineness (m^2/kg)	Specific gravity
19.94	4.76	3.38	1.31	63.93	0.17	0.24	0.44	0.075	0.063	2.54	2.97	360	3.15

where η is the viscosity of the solution, V is the applied voltage, D is the electrode separation, and $\in_m$ is the dielectric constant of the medium.

2.4.3. Optical Microscopy and Image Analysis. In order to monitor the carbon nanotubes and graphene nanoplatelet agglomeration presence in the aqua suspensions and quantify the area of agglomeration, we used optical microscopy. For this purpose, a water suspension drop was analyzed through deposition on a glass plate and covered with a coverslip. Visual inspection was performed with 10x, 20x, and 50x magnifications, while for quantification analysis of the agglomeration area, 10x magnification was used. In this route, three drops were taken as samples from each aqueous suspension; the photos were prepared accurately by microscope software to completely cover the drop area. The samples' optical micrographs were investigated with ImageJ software. The total area of agglomeration was computed by the summation of the total agglomerate area measured for a sample, divided by the total analyzed image area for each drop. The final amount of the agglomeration area was obtained from the average of three drops and expressed as a percentage with standard deviation.

2.5. Characterization of the CNT+GNP Cementitious Composites. Flexural and compressive testing was carried out according to the BS EN 196-1:1995 standard. The apparent porosity, dry bulk density, and capillary water absorption of the samples were measured as stated by ASTM C20, BS EN 1015-10:1999, and BS EN 1015-18 standards. For evaluating the consistency of fresh cementitious composites, the diameters of the paste were measured by using a flow table at two perpendicular directions according to the EN 1015-3 standard. The fracture surfaces of the specimens were characterized by scanning electron microscopy (SEM-FEG, Nano SEM NOVA 200, FEI) using an accelerated voltage of 10 kV and the secondary mode of the electron after coating with an Au-Pd thin film (30 nm), in a high-resolution sputter coater (Cressington 208HR), to investigate the microstructure.

We used a thermogravimetric analyzer (TGA, PerkinElmer) in a nitrogen atmosphere (100 mL/min), at a heating rate of 10°C/min up to 1000°C and energy dispersive X-ray analysis (EDX) with 1.8 nm at 3 kV (Helix detector) of vacuum resolution. The EDX tests were carried out from the cement hydration product accumulation. The graphs were obtained by means of at least five different points of analysis for each specimen. The nondestructive ultrasonic test was performed for microstructural evaluation according to the BS EN 12504-4 standard from Pundit Lab, using the ultrasonic test device H-2984 through two probes along the longitudinal transverse axis. The electrical resistance of the specimens was measured with an Agilent 34461A multimeter, after drying at 34°C for 72 hours. A portable thermal camera, model FLIR 60BX, with a resolution of 320×240 pixels and thermal sensitivity < 0.045°C with a temperature range from -20°C to +650°C was used to evaluate the thermal conductivity of the specimens. Photographs were taken after heating the samples at 70°C for 72 hours. In this route, surface calibration was done before infrared thermography by measuring the emissivity and reflected temperature (ISO 18434-1:2008).

3. Results and Discussion

3.1. Aqueous Suspension Characterization

3.1.1. UV-Visible Spectroscopy. The UV-Vis absorption spectra diagrams for the CNT+GNP suspensions prepared with Pluronic F-127 and SDBS surfactants are displayed in Figures 4 and 5. The dispersion rate of CNT+GNP in liquid suspensions was directly related to the amount of energy absorbance; i.e., a higher energy absorbance indicated a more homogeneous dispersion of CNT+GNP particles within the liquid. Molecules containing bonding and nonbonding electrons (n-electrons) can absorb energy in the form of UV to excite these electrons to higher antibonding molecular orbitals [66]. The more easily the electrons are excited (i.e., a lower energy gap), the longer the wavelength of UV light that is absorbed. The maximum energy absorbances of SDBS and Pluronic suspensions occurred at 275 and 260 nm, respectively. This is likely due to the stronger bonding between Pluronic and CNT+GNP particles, which can guarantee the long-term stability of the liquid suspension.

Parveen et al. [49] also reported similar results for CNT/SDBS and CNT/Pluronic aqueous suspensions through long-term storage stability evaluation. The results also indicate that the increase in the sonication time for both types of surfactants and all concentrations improved the dispersion of the nanoparticles, but at different efficiency levels. The amount of energy absorbed in the SDBS aqueous suspension increased by an average of 17% for each hour of increased sonication time, while for Pluronic, the average was 9%. The sonication time was not increased by more than 3 hours in order to prevent adverse effects on the CNM structural quality, such as edge-type defects, reduction in the aspect ratio, and sp2 domain crystallinity (La), which can cause deleterious influences on the mechanical, electrical, and thermal properties. However, the optimum sonication energy for CNM dispersion can be higher than the 80 W power for 3 hours that was used in this study [67, 68].

Bath sonication dispersing techniques exfoliate GNPs or debundle nanotubes into individual plates or tubes and/or thinner bundles, which consequently are stabilized through electrostatic repulsions and/or the steric force of surfactants. During sonication, mechanical vibrations overcome the van der Waals interactions between the GNPs or bundles of

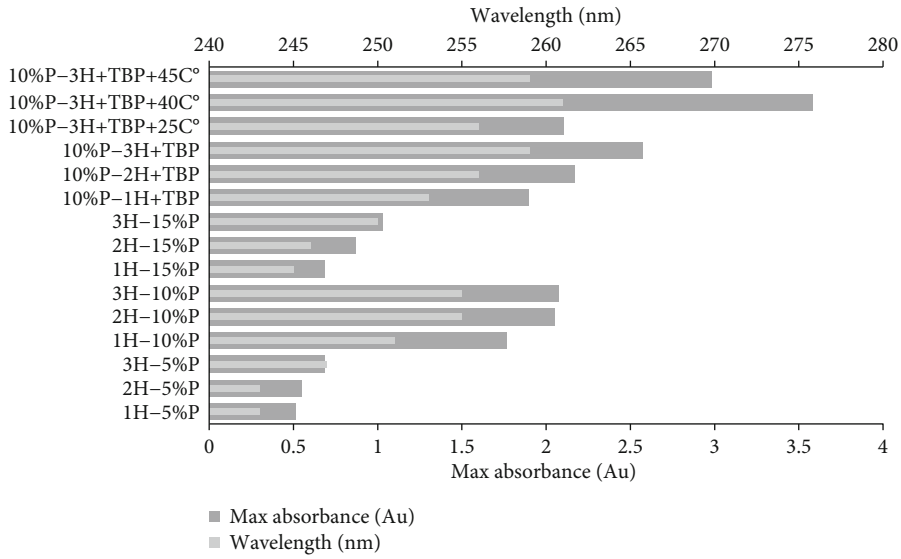

Figure 4: Wavelength and maximum absorbance of CNT+GNP suspensions prepared with Pluronic F-127.

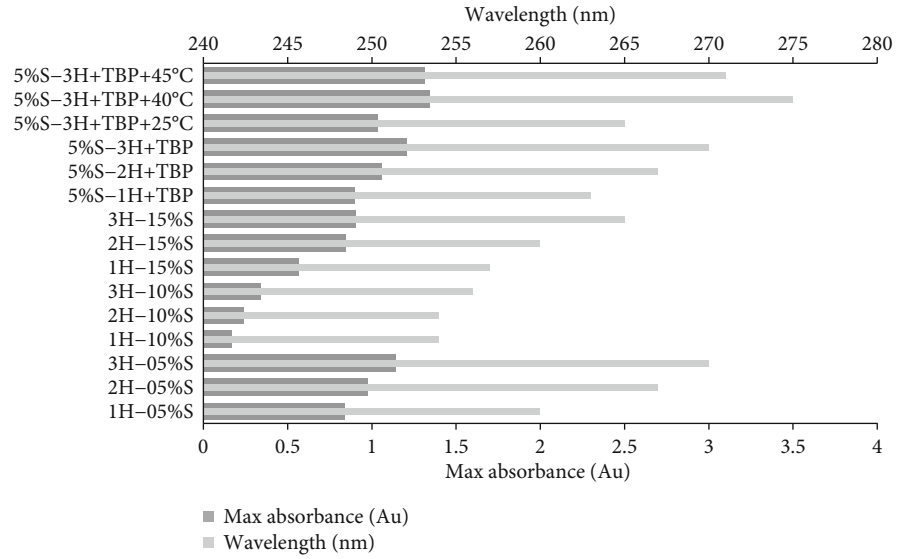

Figure 5: Wavelength and maximum absorbance of CNT+GNP suspensions prepared with SDBS.

CNTs and provide high positional shear, particularly to the end of the GNP sheets or nanotube bundles. Once gaps or spaces at the bundle ends are formed, molecules of the surfactant are absorbed onto the surface of the nanoparticles instantly leading to their exfoliation. According to the unzipping mechanism [69], surfactant molecules have to settle among the small spaces into the bundle to exfoliate the tubes and sheets and to prevent them from reagglomeration.

Hence, short-time ultrasonication in surfactant molecules with bulky hydrophobic groups (Pluronic) showed lower debundling efficiency due to being hindered in their penetration into the intertube or sheet regions. In the case of nonionic surfactants, these bulky hydrophilic groups demonstrated advantages for CNT and/or GNP dispersions likely due to the enhanced steric stabilization caused by longer polymeric groups. The results also demonstrate that an increase in temperature to a certain range (40°C) improved the dispersion of nanoparticles for both suspensions prepared by Pluronic and SDBS, likely by increasing the solvability of the surfactant molecules and the mobility of electrons. However, excessive temperature rises (more than 45°C) caused bond breakage as well as a change in the critical micelle concentration and led to temporary reagglomeration.

In a previous study conducted by Yan et al. [48], a stable and homogeneous aqueous suspension of 0.5% graphene was obtained at a low temperature (25°C) under ultrasonic irradiation with Pluronic F-127. Chen et al. [70] also found that a competent dispersion of graphene (0.56 mg mL^{-1}) could even

be achieved at 165°C in a mixture of N,N-dimethylacetamide and water, via microwave. The results also indicate that the dispersion of CNT+GNP particles was strongly dependent on the surfactant concentration, and the best dispersion occurred with 10% of Pluronic and 5% of SDBS. SDBS is an ionic surfactant while Pluronic is a nonionic surfactant, and their interaction mechanisms with nanocarbon particles are different. In previous studies, Parveen et al. [49] observed that the use of 1% Pluronic for a 0.1% CNT concentration, 5% for 0.2% and 0.3% CNT, and 0.8% SDBS for 0.2% CNT resulted in highly homogeneous CNT dispersions. Yan et al. [48] also achieved a competent aqueous suspension with a 1% Pluronic concentration for 0.5% graphene.

By comparing these results with the present studies, the amount of the required surfactant for dispersing CNT and GNP particles in the hybrid combination appears much greater than the individual cases, in both types of ionic and nonionic surfactants. This is likely due to the combinations of carbon nanoparticles with different geometries (1D and 2D), which leads to an increase in the aspect ratio, as well as the specific surface area. Therefore, in this case, the contact surface between the CNMs was larger than that in the observed CNMs individually, which causes stronger van der Waals attractions and hinders the dispersive efficiency of the surfactant at low concentrations.

The effects of the CNM aspect ratio on the dispersion quality were also demonstrated by Goodman et al. [71] through the investigation of prepared aqueous suspensions with 1 wt% CNTs with a similar length and different diameter, dispersed by alkali lignin (AL), SDS, and CTAB. They observed that the amount of absorbance in the UV-Vis decreased more in the AL suspension when the CNT diameters were decreased from 50 to 8 (nm). These observations revealed that the aspect ratio demonstrated a more prominent effect on the CNT suspensions when AL was used as a surfactant. This reflects the differences in how these molecules adsorb onto the surface of CNMs.

In nonionic surfactants, such as AL and Pluronic, in contrast to ionic surfactants, such as SDS, ASBS, and CTAB, the π-π interactions are responsible for the surfactant molecule adsorption on the CNM surface. The lower aspect ratio of CNMs exhibited a lower surface curvature, which led to a stronger affinity to the -COOH and -OH groups due to a higher overlap between the π electrons. As a result, a higher amount of nonionic surfactant molecules is required for CNM individualization with a high aspect ratio. The interaction type and the nature of the surfactant and, consequently, the concentration are known to play a crucial role in the colloid phase behavior [72] as well as for the nanoparticles [73]. A stabilization mechanism of colloidal type particles is described in the theory of Derjaguin–Landau–Verwey–Overbeek, and this mechanism typically relies on a surface load presence that can be induced by surface group deprotonation or through ion adsorption from the solvent to the colloidal particle surface. A diffuse layer of counterions was attracted by the surface charge from the solvent and formed an electric double layer with a diffuse nature due to the Brownian motion. This can lead to an effective surface charge due to Coulomb repulsion among charged colloidal particles [11].

This mechanism can be applied to GNPs and CNTs by introducing a removable and temporary surface load through permitting the molecules of the surfactant to adsorb via the hydrophobic tails on the nanoparticle surface. An ion normally dissociates itself from the head of hydrophilic groups and serves as a counterion. Then, the adsorbed molecular ions have interactions with water [74]. The active charge signs and magnitude, through the zeta potential, are correlated with the double surface. This is an electrostatic potential of the bound tail group layer edge [11]. For dispersing carbon nanotubes, the concentration of the surfactant has to generally exceed the critical concentration of micelles [75, 76]. The concentration of the surfactant must be higher than the concentration of nanotubes. [11].

Regarding graphene dispersion, the latter condition is not always justified as some surfactants have better performance at concentrations below the critical micelle level while not exceeding the concentration of graphene [76]. The critical micelle concentration in the case of SDBS surfactants may also depend on the nanoparticle concentration [77, 78].

The quality of the dispersion and the individualization/exfoliation degree of GNPs and CNTs are normally measured by the zeta potential. In contrast to carbon nanotubes, this occurs for graphene nanoplatelets within two separate ionic surfactant groups: sulfides, such as SDBS, and other ionic surfactants. Since the zeta potential reflects the electrostatic potential at the edge of the bound ion layers, we assume that maximizing the surface charge in this layer can lead to the zeta potential increase [79]. Hence, the ionic surfactant SDBS with a low molecular weight can pack tightly on the GNP and CNT surface and disperse them with a low concentration.

In Pluronic, as a nonionic surfactant, the lack of Coulomb repulsion for preventing GNP and CNT agglomeration is compensated for by steric effects. Therefore, the main factor determining the dispersibility of CNTs and GNPs in aqueous suspension is the presence of branched and long polar (PEO) chains. This leads to efficiency enhancement by increasing the molecular weight of the surfactant [80]. This occurs due to the surfactant's affinity of π-electrons to the benzene rings of the GNPs and CNTs, which can remain to an extent even after water elimination, in contrast to SDBS (Figure 6).

However, in dry mixes of CNT and GNP without the presence of surfactants, they are arranged in the form of individual spheres without interactions due to the van der Waals attraction forces between the CNTs and repulsion electrostatic forces between the GNPs and CNTs (Figure 2). This is important in the context of carbon nanoparticle refinement and purification from suspensions and can be considered one of the disadvantages of using Pluronic in comparison to SDBS.

3.1.2. Optical Micrograph Analysis. For the evaluation of the agglomerate total area, we analyzed CNT+GNP aqueous suspension optical micrographs and expressed the results as percentages (Table 4). Similar to the previous section, we observed that the dispersion quality was increased by increasing the surfactant concentration up to a certain

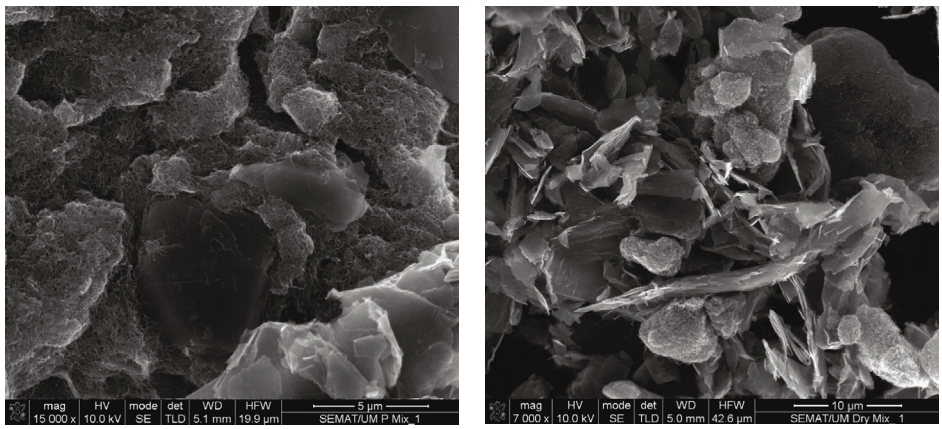

(a) (b)

Figure 6: Morphology of dry CNT+GNP extracted agglomerate from an aqueous suspension: (a) prepared by Pluronic F-127 and (b) prepared by SDBS.

Table 4: Agglomerate total area of various CNT+GNP aqueous suspensions.

SDBS	Total area of agglomerates ± SD (%)	Pluronic F-127	Total area of agglomerates (%)
1%CG-1H-05%S	16.5 ± 0.95	1%CG-1H-5%P	29.6 ± 1.27
1%CG-2H-05%S	11.3 ± 0.61	1%CG-2H-5%P	22.4 ± 0.93
1%CG-3H-05%S	9.1 ± 0.48	1%CG-3H-5%P	18.3 ± 0.81
1%CG-1H-10%S	20.1 ± 1.08	1%CG-1H-10%P	12.3 ± 0.77
1%CG-2H-10%S	16.8 ± 1.1	1%CG-2H-10%P	8.1 ± 0.96
1%CG-3H-10%S	13.3 ± 0.72	1%CG-3H-10%P	3.5 ± 0.62
1%CG-1H-15%S	38.1 ± 1.36	1%CG-1H-15%P	17.4 ± 0.87
1%CG-2H-15%S	32.7 ± 1.09	1%CG-2H-15%P	13.8 ± 0.95
1%CG-3H-15%S	28.3 ± 1.22	1%CG-3H-15%P	10.6 ± 1.14
1%GC-05%S-1H+TBP	12.4 ± 0.84	1%CG − 1H − 10%P + TBP	10.1 ± 1.03
1%GC-05%S-2H+TBP	9 ± 0.73	1%CG − 2H − 10%P + TBP	6.3 ± 0.79
1%GC-05%S-3H+TBP	8.4 ± 0.66	1%CG-3H-10%P+TBP	2.9 ± 0.52
1%GC-05%S-3H+TBP+45°C	6.4 ± 0.71	1%CG-3H-10%P+TBP+45°C	2.1 ± 0.84
1%GC-05%S-3H+TBP+40°C	5.6 ± 0.5	1%CG-3H-10%P+TBP+40°C	1.2 ± 0.71
1%GC-05%S-3H+TBP+25°C	9.1 ± 0.94	1%CG-3H-10%P+TBP+25°C	5.7 ± 0.59
Aqueous suspension without a surfactant			
0.5%CG-1H	88.3 ± 2.37		
0.5%CG-2H	79.1 ± 1.61		
0.5%CG-3H	67.6 ± 1.89		

CG: CNT+GNP (%); S: SDBS (%); P: Pluronic F-127 (%); H: time of sonication (h); ±SD: standard deviation.

level. Beyond this level, a further increase in concentration led to a reduction in the dispersion quality and, consequently, to an increase in the agglomeration area.

Hence, the optimum surfactant concentrations were 15% and 5% for Pluronic and SDBS, respectively, which provided the lower agglomeration area. However, these concentrations were higher than their critical micelle concentrations [49]. Further increases in Pluronic and SDBS concentrations above these optimal values not only represented a surfactant waste but also induced undesired effects. This is consistent with other studies reporting CNT or GNP aqueous dispersions with various types of surfactants [28, 71, 81]. In the

stable aqueous suspensions, a balance is reached between single CNMs and their bundles, which varies with the surfactant concentration. At low concentrations, the surfactant adsorption is limited and does not efficiently counterbalance the van der Waals-induced aggregation of GNPs and CNTs. When the surfactant amounts in the aqueous suspension are above a certain value, large micelles are formed around the bundles of CNMs and they exert an osmotic pressure creating a depletion-induced attraction [82]. Excessively increasing surfactant dosages at higher concentration levels than the critical micelle concentration can lead to nanoparticle reagglomeration due to changing the micelle geometry and even changing the viscosity of the aqueous suspension system. As mentioned before, in similar conditions for sonication, concentration, and temperature, the difference of the dispersion efficiency for different surfactants is closely related to their interactions with CNMs, which depends on the presence of benzene rings, the length of their alkyl chain, and the head group types. At the optimal concentrations, the individualized CNM degree in aqueous suspension is comparable among the various dispersions, with a significant increase on the order of Pluronic > SDBS, as indicated by their respective agglomeration areas.

Interestingly, the presence of TBP enhanced the dispersion of nanoparticles, likely due to the TBP molecular structure that contains three methyl branches. A methyl group is a hydrophobic alkyl functional group derived from methane (CH_4) by removing one hydrogen atom (CH_3-), and methyl groups are extremely reactive and capable of binding covalently with other carbon atoms due to the free capacity of eight radical electrons [83]. However, TBP was added to the suspension as an antifoam agent for removing the bubbles that form on cementitious composites by Pluronic [49].

The optical micrograph analysis also showed the effect of temperature and the increasing sonication time on the nanoparticle dispersion improvement, which was obtained from the UV-visible spectroscopy. The aqueous suspension of 1% CNT+GNP with 10% Pluronic and 3-hour sonication time, at 40°C, with TBP, and the suspension of 5% SDBS with the same amount of TBP, temperature, and sonication time exhibited very low agglomerate areas (only 5.6% and 1.2%, respectively) indicating very competent dispersion qualities (Figure 7). Hence, these suspension systems can be considered to be the optimized suspensions prepared using SDBS and Pluronic. However, compared to the optimized Pluronic suspensions, the suspensions prepared using the optimized percentage of SDBS showed a higher agglomerate area.

3.1.3. Zeta Potential. As mentioned before, the stability of colloidal suspensions is frequently determined by their zeta potential, which indicates the magnitude of the electrostatic interactions between colloidal particles. Particles with a zeta potential higher than +15 mV or less than -15 mV are expected to be stable due to electrostatic considerations. However, colloidal suspensions with zeta potentials between +15 and -15 mV can also be stable if they are stabilized uninterruptedly [64].

The zeta potentials of the CNT+GNP suspensions are listed in Table 5.

The dispersions of 1% CNT+GNP in 5%, 10%, and 15% SDBS with 3-hour sonication showed zeta potentials of -48.6, -17.7, and -29 (mV), respectively. However, these amounts for Pluronic suspensions were approximately -2.9, -9.3, and -5.7 (mV), respectively. The addition of 5% of TBP over SDBS, with 3-hour sonication, obtained a -56.4 (mV) zeta potential, which supports the positive effect of TBP to improve CNT and GNP dispersion. Increasing the temperature to 40°C led to increasing the zeta potential to -71.9 (mV), which shows more colloidal particle stability for this suspension. However, the excessive increase in temperature decreased the quality of the CNM dispersion. Similarly, increasing the temperature up to 40°C for the 10% Pluronic prepared through 3-hour sonication with TBP led to the formation of more stable colloidal particles with a -23.1 (mV) zeta potential.

The high negative zeta potential for SDBS suspensions is due to the high negative surface charges of this surfactant. Consequently, due to the nonionic chemical structure of Pluronic, the CNT+GNP suspensions prepared by this surfactant presented lower negative zeta potential. Owing to nonelectrostatic and steric interactions, the Pluronic suspensions could also be stable. The polyoxyethylene (PEO) hydrophilic groups extend into the water while hydrophobic chains of polyoxypropylene (PPO) interact with the surfaces of the GNPs and CNTs. The exfoliation and stabilization of separated GNPs and CNTs happen as a result of steric hindrances that were induced by the long PEO chain.

The functionalized CNM zeta potential was relatively higher due to -COOH functional groups, which leads to the surface negative charge on GNPs and CNTs.

3.1.4. The Average CNT+GNP Bundle Size. The average size of the CNM bundles and the polydispersity index (PDI) of the CNT+GNP suspensions, determined through DLS by measuring the hydrodynamic diameter, are presented in Table 6. The PDI is used as a scale to indicate the extent of the particle size distribution range, and the larger PDI demonstrates the wider molecular size spectrum. The results indicate that the particle sizes of CNT+GNP suspensions dispersed in 5%, 10%, and 15% Pluronic and SDBS were around 512, 328, and 389 nm and 491, 671, and 588 nm, respectively, which shows an optimum concentration around 10% for Pluronic and 5% for SDBS, as discussed before.

The small average size of CNM bundles in Pluronic suspensions, in comparison with SDBS ones, indicates the efficiency of the -COOH functional groups on the unbundling process. A lower particle size (219 nm) and lower PDI (0.315) were obtained for 10% of Pluronic, with 3-hour sonication with TBP at 40°C, showing low agglomeration and high quality of the dispersion. The average particle size and the amount of PDI in the SDBS-dispersed suspensions, at optimum conditions, were around 393 nm and 0.462, respectively.

3.2. Cementitious Composite Characterization

3.2.1. Mechanical Microstructural Behavior. After obtaining the best dispersed mixed design for hybrid CNT+GNP

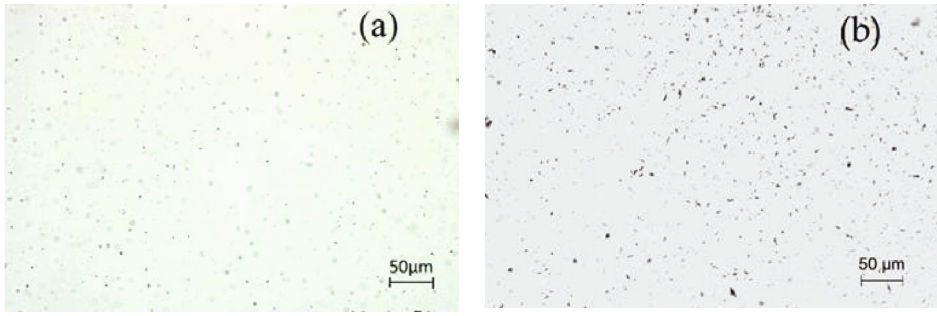

(a) (b)

Figure 7: Optical micrographs of CNT/GNP suspensions: (a) Pluronic: 1%CG-3H-10%P+TBP+40°C; (b) SDBS: 1% CG-3H-5%S+TBP +40°C.

Table 5: Zeta potentials of the CNT+GNP suspensions.

Sample name	Zeta potential (mV)
3H-05%S	-48.6
3H-10%S	-17.7
3H-15%S	-29
5%S-3H+TBP	-56.4
5%S-3H+TBP+25°C	-35.5
5%S-3H+TBP+40°C	-71.9
5%S-3H+TBP+45°C	-67.3
3H-5%P	-2.9
3H-10%P	-9.3
3H-15%P	-5.7
3H-10%P+TBP	-14.6
3H-10%P+TBP+25°C	-13.1
3H-10%P+TBP+40°C	-23.1
3H-10%P+TBP+45°C	-19.9

Table 6: The CNM hydrodynamic diameters in different suspensions characterized by DLS.

Sample name	Ave bundle size (nm)	PDI
3H-05%S	491	0.571
3H-10%S	671	0.707
3H-15%S	588	0.649
5%S-3H+TBP	448	0.514
5%S-3H+TBP+25°C	474	0.589
5%S-3H+TBP+40°C	393	0.462
5%S-3H+TBP+45°C	422	0.503
3H-5%P	512	0.576
3H-10%P	328	0.488
3H-15%P	389	0.51
3H-10%P+TBP	296	0.412
3H-10%P+TBP+25°C	311	0.438
3H-10%P+TBP+40°C	219	0.315
3H-10%P+TBP+45°C	287	0.397

aqueous suspensions with each surfactant, the mechanical and microstructural properties of the reinforced cementitious composites were evaluated to determine their effects. The mechanical and microstructural parameters of the cementitious composites in different cases are shown in Figure 8 and Table 7. The results were obtained as the means of at least three specimens for each test performed. Reinforcing the cementitious composites with CNT+GNP/Pluronic suspensions led to a higher bulk density compared to CNT +GNP/SDBS. Consequently, the time required for an ultrasonic wave to pass and the apparent porosity values of the CNT+GNP/Pluronic-reinforced specimens were lower than those of the CNT+GNP/SDBS specimens.

The general trend of the results showed an improvement in the flexural and compressive strength of CNT +GNP/Pluronic-incorporated cementitious mortars. These results demonstrate more homogeneous and denser microstructures for the CNT+GNP/Pluronic-reinforced cementitious composites. The positive effects of the CNTs and GNPs on the improvement of the cementitious composite microstructures and their mechanical behaviors, including their flexural and compressive strength, have been reported in many previous studies [84–86]. The unique features of these 1D and 2D nanomaterials with high aspect ratios enhance the microstructural and the mechanical properties of the cementitious composites, generally, by reducing the microporosities, accelerating the hydration process, and bridging the cement hydration product mechanism, which is highly controlled by the CNM aspect ratio and dispersion technique [6, 87, 88].

Therefore, we concluded that the differences between the cementitious composite mechanical and microstructure parameters in the cases of CNT+GNP/Pluronic and CNT +GNP/SDBS were due to the dispersion quality and the secondary effects of the surfactant on the hydration process and/or on the nanoparticle features and/or structures. However, considering the mechanical and microstructural results for the nonreinforced composites prepared with only Pluronic and SDBS (without CNMs), the presence of these two surfactants did not demonstrate adverse effects on the cementitious composite features, at least after 28 days of hydration and for the tested concentrations.

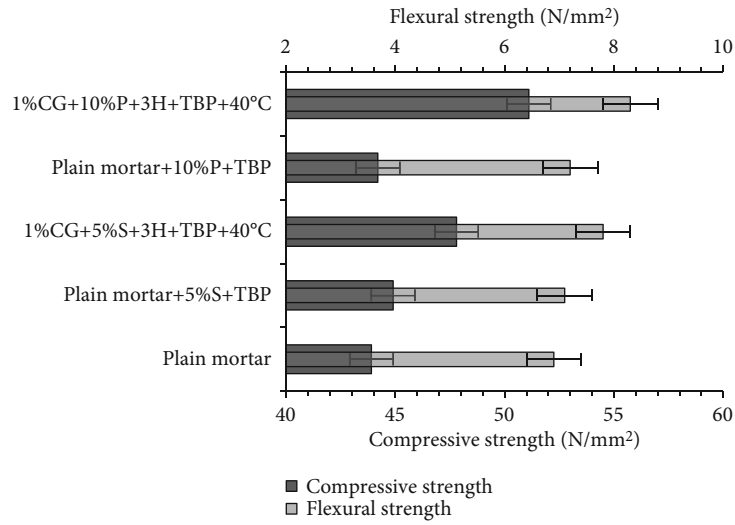

Figure 8: The compressive and flexural strength of cementitious composites after 28 days of hydration.

Table 7: Test results of the cementitious composites according to the standard procedures.

Name of sample	Flow values[1] (mm)	Flexural strength[2] (N/mm^2)	Compressive strength[2] (N/mm^2)	Apparent porosity[3] (%)	Ultrasonic wave time passing[4] (μs) for 150 kHz Longitudinal	Transverse	Dry bulk density[5] (kg/m^3)
Plain mortar	183.2	6.9	43.9	19	36.40	9.70	2125
Plain mortar+5%S +TBP	191.7	7.1	44.9	15.9	36.21	9.51	2130
1%CG+5%S+3H +TBP+40°C	118.4	7.8	47.8	13.6	34.10	9.34	2135
Plain mortar +10%P+TBP	198.2	7.2	44.2	13.9	35.88	9.38	2130
1%CG+10%P+3H +TBP+40°C	131.5	8.3	51.1	11.4	32.97	8.93	2140

[1]BS EN 1015-3; [2]BS EN 196-1:1995; [3]ASTM C20; [4]BS EN 12504-4; [5]BS EN 1015-10:1999.

Large agglomerations of CNTs and GNPs, due to lower quality dispersions in CNT+GNP/SDBS-reinforced cementitious composites, led to the formation of microporosities. The CNM agglomerated between the growing units of C-S-H to create large gaps among them, which prevented their physical connection (Figure 9(a)). This is especially important for the GNPs, which are larger in size. As can be seen in Figure 10, the CNTs showed a higher reinforcement capacity to improve the bridging behavior for the pull-out strength with a better dispersion. The presence of large GNP agglomerates between the hydration products produced a nanoscale discontinuity when applying stress, which may facilitate the formation of microcracks.

However, well-dispersed GNPs were more able to anchor the neighboring C-S-H clusters and bridge the voids between them. The large specific surface area of GNPs led to a high contact area with the hydration products and maximized the stress transferring, delaying the microcrack and macrocrack propagation. In contrast to SDBS, the CNT +GNP/Pluronic-reinforced cementitious composites contained lower porosities due to the better dispersion of the nanoparticles.

The results of the capillary water absorption shown in Figure 11 also emphasize this. According to the slope of the capillarity result graphs, the rates of capillarity water absorption in the GNP+CNT/Pluronic-reinforced specimens were significantly lower than those in the GNP+CNT/SDBS specimens.

However, the rates of capillary water absorption for CNT +GNP-reinforced composites prepared by both Pluronic and SDBS were lower than those for the plain composite.

The presence of both surfactants increased the flowability of the plain mortar. According to Table 7, the flow values of the specimen with 10% individual Pluronic increased by 9% and 5%, respectively, compared to those of the SDBS and the plain cases. The chemical structure of Pluronic F-127 contains hydrophilic PEO (polypropylene oxide) side chains similar to commonly used superplasticizers of polycarboxylate, as mentioned before. Polypropylene oxide side chains were reported to be the main chemical components of these

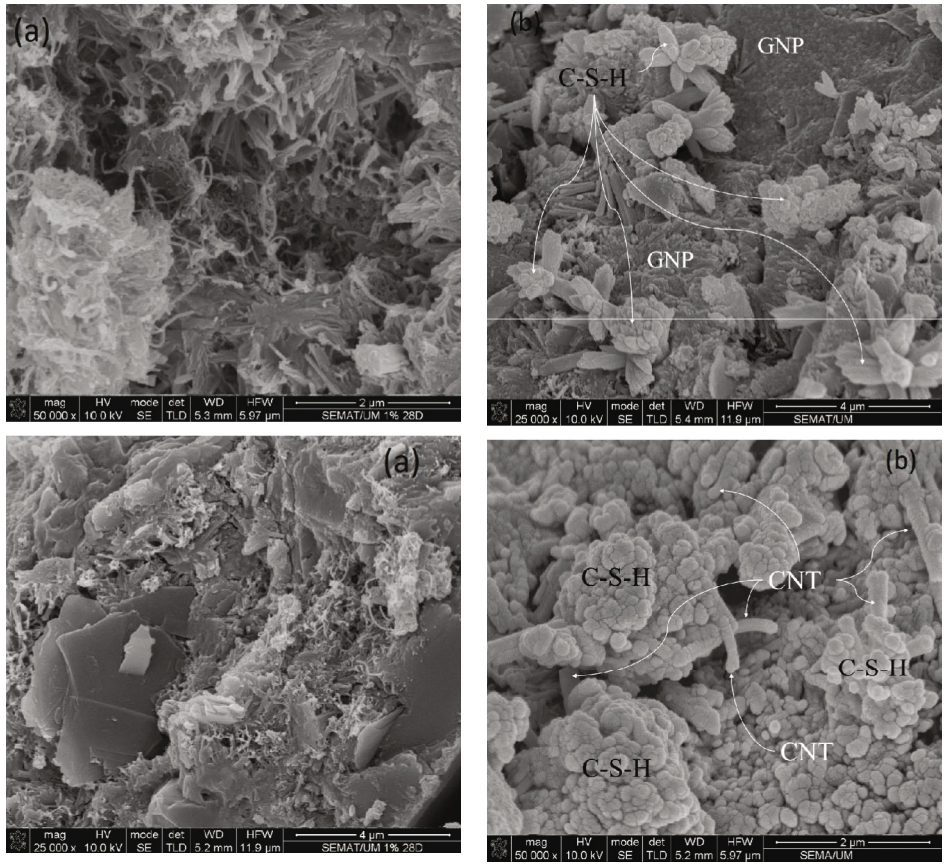

(a) (b)

Figure 9: SEM morphology of cementitious composites reinforced by (a) CNT+GNP/SDBS or (b) CNT+GNP/Pluronic.

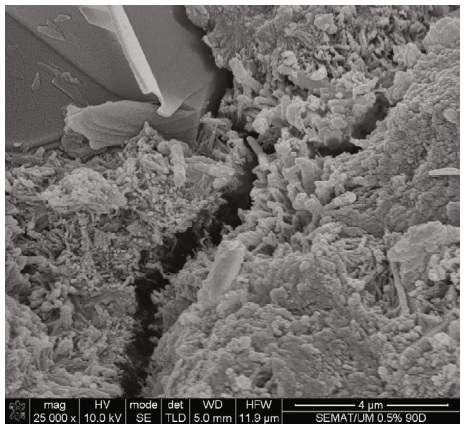

Figure 10: SEM morphology of a CNT+GNP/SDBS sample after the mechanical strength measurement.

superplasticizers that are responsible for the cement particle dispersion and the improvement of the flowability [89].

It is generally accepted that the cement paste fluidity is directly pertinent for the performance of hardened cement (such as the pore structure and strength) [90]. However, the presence of CNT and GNP reduced the flowability of cementitious composites [49, 50]. Due to the large surface area of GNPs and CNTs, they can absorb water molecules; hence, a significant reduction occurred in the free water content needed for lubrication, and this led to a reduction in the fluidity. For this reason, the flowability of CNT+GNP-reinforced samples prepared with Pluronic and SDBS decreased by 27% and 36% compared to that of the plain cementitious composite, respectively.

Generally, cement hydration products have a strong tendency to form on the surface of CNTs and GNPs due to the large specific surface area accompanied by a high amount of oxygen functional groups, which serve as nucleation sites [15, 91]. Although the hydration C_3S and C_2S produce C-S-H gel and C-H crystals, any deficiency in the water content surrounding these silicates can slow down the hydration reactions [91]. This is especially true around agglomerates caused by the lower quality of dispersion (Figure 9(a)).

High-magnification SEM images (Figure 9(b)) of the reinforced cementitious composite with CNT+GNP/Pluronic investigated by EDX tests indicate that CNTs and GNPs were embedded appropriately within the hydration products, in contrast to the CNT+GNP/SDBS-reinforced specimens. This is due to the higher quality of the dispersion and the presence of the PEO side chains, which are preferentially adsorbed on the surfaces of the C-S-H gel as well as along the CNT lengths and GNP surfaces [91]. In the early periods of hydration, this causes a slight discoloration of the graphene and increases the CNT diameters due to the extremely

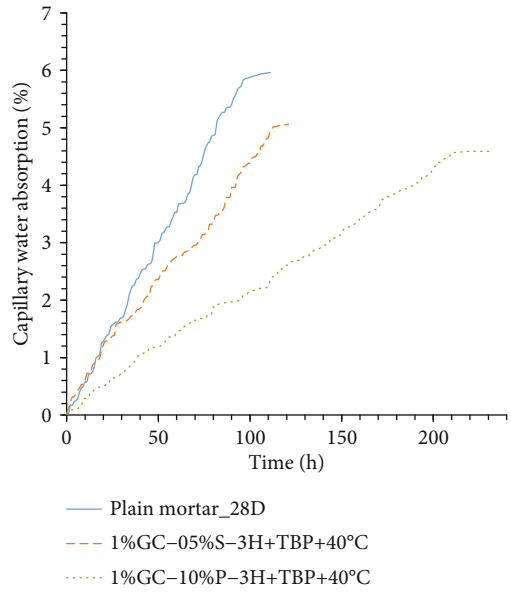

Figure 11: Capillary water absorption of cementitious composites.

thin layer of hydration product coating (in the form of pollen). Over time, the crystals become thicker and the carbon nanoparticles become completely embedded in them.

The results of thermogravimetric analysis (TGA) and differential scanning calorimetry (DSC) for different cementitious cases are shown in Figure 12. From the TGA curve, the first decay is observed up to 105°C, which can be attributed to the removal of the moisture and free water of the cementitious composite samples. The second decay was observed between 105 and 400°C, due to the dehydration of the chemically bonded water existing in the hydrates, i.e., ettringite, carboaluminates, and C-S-H. The next major decay was found between 400 and 550°C, which can be attributed to the dehydroxylation of CH. Fourth, the last decay was ascribed to calcium carbonate coming from the clinker and cementitious composite carbonation, which was observed between 600 and 800°C [92, 93].

The results indicate that the amounts of hydration products in the CNT+GNP/Pluronic-reinforced specimens were more than those in the CNT+GNP/SDBS specimens; however, the hydration product amounts in both cases were more than those in the plain sample.

In the case of the reinforced cementitious composites with MWNTs, Konsta-Gdoutos et al. [94, 95] reported similar findings. They observed, by nanoindentation tests, that multiwall carbon nanotubes could increase the formation of a larger amount of high-stiffness calcium silicate hydrate gel and decrease the nanoscale porosity owing to the gap filling between gels of C-S-H through CNTs. Therefore, based on the results of the previous research [88] and from the present study, one of the major effects of nanoparticles in the cementitious composite is to increase the hydration rate. The energy-dispersive X-ray spectroscopy (EDX) results for cementitious composites are shown in Figure 13. These results were obtained from the mean of five different points of cement hydration product accumulation for each case.

Despite higher carbon concentration in the place of cement hydration product accumulation for CNT +GNP/SDBS-reinforced specimens compared to CNT +GNP/Pluronic specimens, lower amounts of hydration products were observed. The reason for this is likely the changing nanoparticle features and/or structures due to the SDBS dispersion mechanism. This statement could be verified by evaluating the electrical behavior.

3.2.2. Electrical Resistance. The electrical resistances of specimens after 28 days of hydration were measured using a digital multimeter (Table 8). Since humidity, as an electrically conductive factor, has a relatively significant effect on the cementitious specimen electrical resistance changes [96, 97], the electrical resistance was measured after drying the specimens at 34°C for 72 hours. The electrical resistances of individual CNT- and GNP-reinforced specimens were also measured using a similar method in order to compare with that of hybrid CNT+GNP.

The electrical resistances of the reinforced specimens with CNT+GNP/SDBS, CNT/SDBS, and GNP/SDBS were improved by 71.73%, 66%, and 53.2%, respectively, in comparison to that of the plain mortar, while the results are 60.94%, 70.3%, and 64.3%, respectively, for the Pluronic-reinforced specimens. According to the previous section's discussion, CNT+GNP/SDBS-reinforced specimens contained more and larger CNM agglomerations compared to CNT+GNP/Pluronic specimens due to the lower dispersion quality. Although the existence of a certain agglomeration quantity can act as a key factor in raising the conductivity significantly and reducing the percolation threshold value [11], the cementitious composite reinforced with CNT +GNP/Pluronic showed higher electrical conductivity.

Therefore, the decreasing electrical conductivity of the CNT+GNP/SDBS-reinforced composites is likely due to the nanoparticle features and/or structure changes provided by the SDBS dispersion mechanism.

In previous studies, significant deterioration in the electrical properties was also reported due to disturbances of the graphene/CNT surface π-electron delocalization.

The synergic effects of hybrid CNT+GNP specimens decreased the electrical resistance of the cementitious composites more than what was observed for individual CNT or GNP utilization, as was expected.

A comparison of the CNT+GNP effects on the electrical conductivity of cementitious composites with previous studies that used individual CNT, graphene, or other carbon-based particles (Table 9) clearly indicated that the hybrid combination of CNTs and GNPs was more efficient to create a conductive path among the cementitious composites as was expected. This combination can reduce the percolation threshold and enhance the quantum tunneling effect due to the 1D and 2D geometrical shapes.

3.2.3. Thermal Photography. In this study, for the first time, thermal photography was used for the evaluation of CNT +GNP dispersion in hardened specimens through the difference between the thermal diffusion coefficient and the thermal conductivity. Thermal photography of cementitious

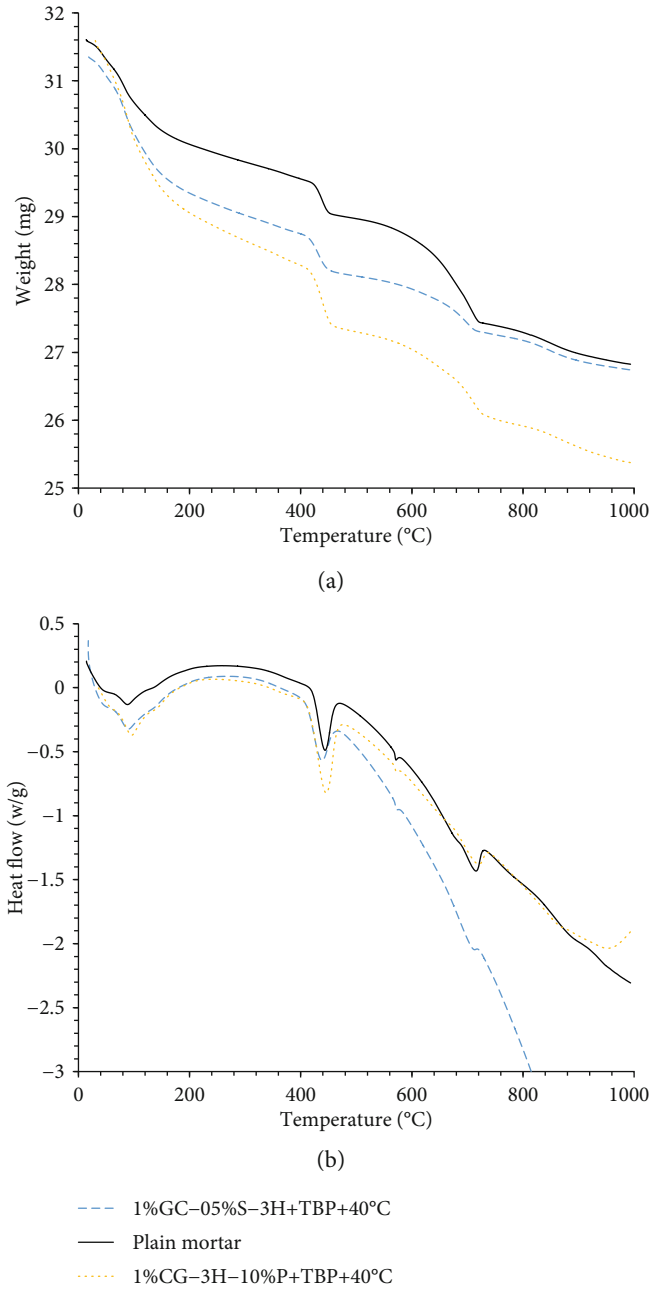

Figure 12: Thermal analysis of the cementitious composite: (a) TGA analysis and (b) DSC analysis.

composite specimens of the same size (160 mm × 40 mm × 40 mm) in different periods of cooling time is shown in Figure 14, after heating to 70°C, for 72 hours. As expected, reinforced CNT+GNP cementitious composite samples absorbed more heat due to the high thermal conductivity [98]. They also lost heat more rapidly over time due to the high thermal transfer coefficient compared to the plain composites. As shown in Figures 14(a) and 14(b), the CNT +GNP/Pluronic-reinforced specimens lost heat more rapidly in comparison to the CNT+GNP/SDBS specimens. This was likely due to disturbances in the delocalization of π-electrons on the nanoparticle surfaces, which were caused by the SDBS dispersion mechanism. This verifies the previous results. Nonhomogeneous heat distribution caused by considerable large agglomerations on CNMs for CNT+GNP/SDBS composites indicated the inappropriate dispersion of nanoparticles in the hardened sample, as discussed before.

4. Conclusion

In this work, we conducted an extensive experimental research study on hybrid CNT+GNP dispersion techniques using a high concentration of noncovalent surfactants and aqueous suspensions. For this purpose, a nonionic Pluronic F-127 and ionic SDBS surfactants were studied in 1 wt% of CNT+GNP (0.5% CNT and 0.5% GNP) dispersions,

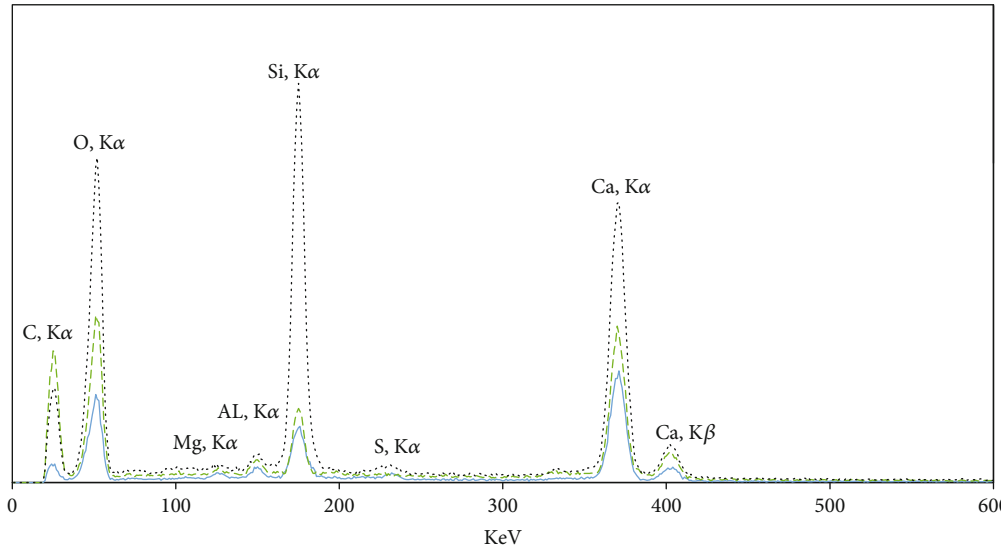

Samples	Elements (wt%)						
	C	O	Mg	AL	Si	S	Ca
Plain mortar	1.7	17.6	7.7	1.1	21.9	6.3	43.7
1%GC–05%S–3H+TBP+40°C	21.2	20.2	6.4	0.9	14.1	5.4	31.8
1%CG–3H–10%P+TBP+40°C	10.2	32.9	0.5	0.7	22.9	0.5	32.3

Figure 13: Energy-dispersive X-ray spectroscopy (EDX) of cementitious composites and their normalized elemental analysis.

Table 8: The electrical resistance and humidity of cementitious composite specimens.

Sample	Electrical resistance (Ω)	Improvement (%)	Moisture (%)
Plain mortar	8446.00	—	8.90
1%GC-5%S-3H+TBP+40°C	2388.00	71.73	6.78
1%CNT-5%S-3H+TBP+40°C	2847	66	7.7
1%GNP-5%S-3H+TBP+40°C	3949	53.2	8.04
1%GC-10%P-3H+TBP+40°C	765.00	90.94	4.97
1%CNT-10%P-3H+TBP+40°C	2506	70.3	6.2
1%GNP-10%P-3H+TBP+40°C	3011	64.3	7.93

Table 9: Comparison of the electrical resistances for carbon nanoparticle-reinforced cementitious composites.

Dispersion method	Weight fraction (%)	Nanoparticle type	Electrical resistivity (Ω·m)	References
Superplasticizer and ultrasonication	5	GNP	21.02	[10]
Dry mechanical mixing	5	GNP	78.20	[10]
Superplasticizer and high-speed mixer	5	GNP	27.96	[10]
PVP and ultrasonication	0.7	CNT	24	[99]
Mixing by superplasticizer during mortar blending	10	Carbon black	4.53	[100]
Mixing by superplasticizer during mortar blending	2	Short carbon fiber	2.4	[101]
Pluronic F-127 and TBP, 3 h sonication, 40°C	1 (half by half)	GNP+CNT	15.3	Present study
SDBS and TBP, 3 h sonication, 40°C	1 (half by half)	GNP+CNT	47.76	Present study

to analyze the effect of factors, including the surfactant concentration, sonication time, temperature, and the use of an antifoam agent (TBP).

We evaluated the effects of optimized CNT+GNP suspensions prepared by SDBS and Pluronic on the mechanical, electrical, and thermal properties of cementitious composites by various tests. UV-spectroscopy and optical microscopy image analysis indicated that high-quality CNT+GNP dispersions with a low agglomeration area (less than 1.2%) were achieved with 10% Pluronic (wt% of nanoparticles), with 3-hour

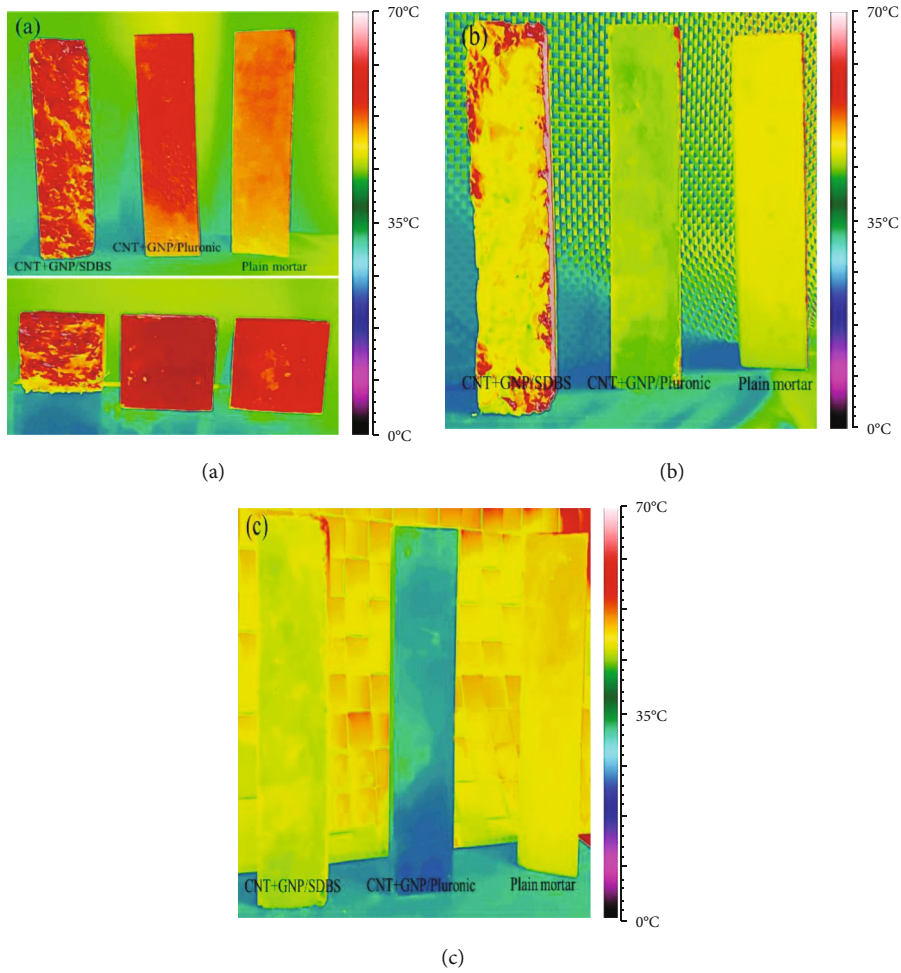

(a) (b) (c)

Figure 14: Thermography of cementitious composites at different times: (a) immediately after heating (both cross section and side view), (b) after one hour, and (c) after two hours.

sonication, at 40°C, with the presence of tributyl phosphate (50 wt% of the surfactant as an antifoam agent). The optimum percentage of SDBS (5 wt%) led to a lower dispersion quality and a higher agglomeration area (5.6%).

Increasing the temperature up to 40°C, as mentioned before, played a positive role in the dispersion of suspensions prepared with Pluronic or SDBS; however, higher temperatures led to the reagglomeration of CNT+GNP. The presence of TBP significantly reduced the agglomeration area. Increasing the sonication time improved the dispersion in both CNT +GNP/Pluronic and CNT+GNP/SDBS aqueous suspensions, which was also confirmed by the zeta potential and particle size measurements. SEM photographs showed that CNTs and GNPs in prepared aqueous suspensions using Pluronic presented better interactions between each other, even after water elimination, when compared to CNT+GNP/SDBS suspensions.

Cementitious composites reinforced with hybrid CNT +GNP showed enhanced mechanical, microstructural, electrical, and thermal properties, for both the Pluronic and SDBS dispersion cases. However, the general result trends demonstrate higher efficiency for CNT+GNP/Pluronic due to the compatible mechanism and the dispersion quality.

The results obtained for the dry bulk density, water content, ultrasonic nondestructive test, and capillarity water absorption also indicate denser microstructures for the CNT+GNP/Pluronic-reinforced composites due to the lower agglomeration caused by the high-quality dispersion. The TGA, DSC, and EDX results show that dispersed CNT +GNP/Pluronic increased the hydration rate due to the nucleation agent effects of CNTs and GNPs and the oxygen functional groups of graphene, which acted as growing points for hydration products. SEM image analysis showed that CNMs were completely embedded in the hydration products, bridging them. However, this is not observed for CNT +GNP/SDBS due to the lower quality dispersion and also to the changing CNM features and structures caused by the SDBS dispersion mechanism. For the same reason, CNT +GNP/SDBS-reinforced specimens also presented lower electrical and thermal conductivities compared to those reinforced with CNT+GNP/Pluronic.

Data Availability

Requests for all types of data used to support the findings of this study, after the publication of this article, will be

considered by the corresponding author, subject to obtaining permission from the owners.

Conflicts of Interest

The authors declare that they have no conflicts of interest.

Acknowledgments

This work was supported by the European Commission-Shiff2Rail Program under the project "IN2TRACK2–826255-H2020-S2RJU-2018/H2020-S2RJU CFM-2018." The authors are thankful to Gonzalo Mármol, Paulo Lopes, Vânia Pais, and Rui Rodrigues for their inputs to analyze the experimental results.

References

[1] D. Zhuo, R. Wang, L. Wu et al., "Flame Retardancy Effects of Graphene Nanoplatelet/Carbon Nanotube Hybrid Membranes on Carbon Fiber Reinforced Epoxy Composites," *Journal of Nanomaterials*, vol. 2013, no. 7, 7 pages, 2013.

[2] B. Han, S. Sun, S. Ding, L. Zhang, X. Yu, and J. Ou, "Review of nanocarbon-engineered multifunctional cementitious composites," *Composites Part A: Applied Science and Manufacturing*, vol. 70, pp. 69–81, 2015.

[3] Z. Li, S. Ding, X. Yu, B. Han, and J. Ou, "Multifunctional cementitious composites modified with nano titanium dioxide: a review," *Composites Part A: Applied Science and Manufacturing*, vol. 111, pp. 115–137, 2018.

[4] M. Li, V. Lin, J. Lynch, and V. C. Li, "Multifunctional carbon black engineered cementitious composites for the protection of critical infrastructure," in *High Performance Fiber Reinforced Cement Composites 6: HPFRCC 6*, G. J. Parra-Montesinos, H. W. Reinhardt, and A. E. Naaman, Eds., pp. 99–106, Springer Netherlands, Dordrecht, 2012.

[5] X. J. Wang, D. L. Zhao, D. D. Zhang, C. Li, and R. R. Yao, "Remarkable mechanical and thermal increments of epoxy composites by graphene nanosheets and carbon nanotubes synergetic reinforcement," *Key Engineering Materials*, vol. 727, pp. 546–552, 2017.

[6] S. Chuah, Z. Pan, J. G. Sanjayan, C. M. Wang, and W. H. Duan, "Nano reinforced cement and concrete composites and new perspective from graphene oxide," *Construction and Building Materials*, vol. 73, pp. 113–124, 2014.

[7] A. K. Geim and K. S. Novoselov, "The rise of graphene," *Nature Materials*, vol. 6, no. 3, pp. 183–191, 2007.

[8] S.-Y. Yang, W.-N. Lin, Y.-L. Huang et al., "Synergetic effects of graphene platelets and carbon nanotubes on the mechanical and thermal properties of epoxy composites," *Carbon*, vol. 49, no. 3, pp. 793–803, 2011.

[9] W. Li, A. Dichiara, and J. Bai, "Carbon nanotube–graphene nanoplatelet hybrids as high-performance multifunctional reinforcements in epoxy composites," *Composites Science and Technology*, vol. 74, pp. 221–227, 2013.

[10] O. E. Ozbulut, Z. Jiang, and D. K. Harris, "Exploring scalable fabrication of self-sensing cementitious composites with graphene nanoplatelets," *Smart Materials and Structures.*, vol. 27, no. 11, p. 115029, 2018.

[11] E. E. Tkalya, M. Ghislandi, G. de With, and C. E. Koning, "The use of surfactants for dispersing carbon nanotubes and graphene to make conductive nanocomposites," *Current Opinion in Colloid & Interface Science*, vol. 17, no. 4, pp. 225–232, 2012.

[12] V. C. Li, "High-performance and multifunctional cement-based composite material," *Engineering*, vol. 5, no. 2, pp. 250–260, 2019.

[13] Y.-M. Jen and J.-C. Huang, "Synergistic effect on the thermomechanical and electrical properties of epoxy composites with the enhancement of carbon nanotubes and graphene nano platelets," *Materials*, vol. 12, no. 2, p. 255, 2019.

[14] S. Chatterjee, F. Nafezarefi, N. H. Tai, L. Schlagenhauf, F. A. Nüesch, and B. T. T. Chu, "Size and synergy effects of nanofiller hybrids including graphene nanoplatelets and carbon nanotubes in mechanical properties of epoxy composites," *Carbon*, vol. 50, no. 15, pp. 5380–5386, 2012.

[15] S. Lv, Y. Ma, C. Qiu, T. Sun, J. Liu, and Q. Zhou, "Effect of graphene oxide nanosheets of microstructure and mechanical properties of cement composites," *Construction and Building Materials*, vol. 49, pp. 121–127, 2013.

[16] S. Parveen, S. Rana, and R. Fangueiro, "A Review on Nanomaterial Dispersion, Microstructure, and Mechanical Properties of Carbon Nanotube and Nanofiber Reinforced Cementitious Composites," *Journal of Nanomaterials*, vol. 2013, Article ID 710175, 9 pages, 2013.

[17] M.-Y. Shen, T.-Y. Chang, T.-H. Hsieh et al., "Mechanical Properties and Tensile Fatigue of Graphene Nanoplatelets Reinforced Polymer Nanocomposites," *Journal of Nanomaterials*, vol. 2013, Article ID 565401, 9 pages, 2013.

[18] J.-L. Phua, P.-L. Teh, S. A. Ghani, and C.-K. Yeoh, "Effect of Heat Assisted Bath Sonication on the Mechanical and Thermal Deformation Behaviours of Graphene Nanoplatelets Filled Epoxy Polymer Composites," *International Journal of Polymer Science*, vol. 2016, 8 pages.

[19] A. Ibrahim, S. Ridha, A. Amer, R. Shahari, and T. Ganat, "Influence of Degree of Dispersion of Noncovalent Functionalized Graphene Nanoplatelets on Rheological Behaviour of Aqueous Drilling Fluids," *International Journal of Chemical Engineering*, vol. 2019, Article ID 9767183, 11 pages, 2019.

[20] S.-T. Kang, J.-Y. Seo, and S.-H. Park, "The Characteristics of CNT/Cement Composites with Acid-Treated MWCNTs," *Advances in Materials Science and Engineering*, vol. 2015, 9 pages, 2015.

[21] L. I. Nasibulina, I. V. Anoshkin, A. G. Nasibulin, A. Cwirzen, V. Penttala, and E. I. Kauppinen, "Effect of carbon nanotube aqueous dispersion quality on mechanical properties of cement composite," *Journal of Nanomaterials*, vol. 2012, no. 6, Article ID 169262, 6 pages, 2012.

[22] B. Munkhbayar, M. J. Nine, J. Jeoun, M. Bat-Erdene, H. Chung, and H. Jeong, "Influence of dry and wet ball milling on dispersion characteristics of the multi-walled carbon nanotubes in aqueous solution with and without surfactant," *Powder Technology*, vol. 234, pp. 132–140, 2013.

[23] A. H. Korayem, M. R. Barati, S. J. Chen, G. P. Simon, X. L. Zhao, and W. H. Duan, "Optimizing the degree of carbon nanotube dispersion in a solvent for producing reinforced epoxy matrices," *Powder Technology*, vol. 284, pp. 541–550, 2015.

[24] X.-L. Jia, Q. Zhang, J.-Q. Huang, C. Zheng, W.-Z. Qian, and F. Wei, "The direct dispersion of granular agglomerated carbon nanotubes in bismaleimide by high pressure

homogenization for the production of strong composites," *Powder Technology*, vol. 217, pp. 477–481, 2012.

[25] S. J. Chen, C. Y. Qiu, A. H. Korayem, M. R. Barati, and W. H. Duan, "Agglomeration process of surfactant-dispersed carbon nanotubes in unstable dispersion: a two-stage agglomeration model and experimental evidence," *Powder Technology.*, vol. 301, pp. 412–420, 2016.

[26] M. D. Clark, S. Subramanian, and R. Krishnamoorti, "Understanding surfactant aided aqueous dispersion of multi-walled carbon nanotubes," *Journal of Colloid and Interface Science.*, vol. 354, no. 1, pp. 144–151, 2011.

[27] M. Bystrzejewski, A. Huczko, H. Lange, T. Gemming, B. Büchner, and M. H. Rümmeli, "Dispersion and diameter separation of multi-wall carbon nanotubes in aqueous solutions," *Journal of Colloid and Interface Science*, vol. 345, no. 2, pp. 138–142, 2010.

[28] R. Rastogi, R. Kaushal, S. K. Tripathi, A. L. Sharma, I. Kaur, and L. M. Bharadwaj, "Comparative study of carbon nanotube dispersion using surfactants," *Journal of Colloid and Interface Science*, vol. 328, no. 2, pp. 421–428, 2008.

[29] J.-Y. Shin, T. Premkumar, and K. . E. Geckeler, "Dispersion of single-walled carbon nanotubes by using surfactants: are the type and concentration important?," *Chemistry - A European Journal*, vol. 14, no. 20, pp. 6044–6048, 2008.

[30] A. J. Blanch, C. E. Lenehan, and J. S. Quinton, "Optimizing surfactant concentrations for dispersion of single-walled carbon nanotubes in aqueous solution," *The Journal of Physical Chemistry B*, vol. 114, no. 30, pp. 9805–9811, 2010.

[31] J. U. Lee, J. Huh, K. H. Kim, C. Park, and W. H. Jo, "Aqueous suspension of carbon nanotubes via non-covalent functionalization with oligothiophene-terminated poly(ethylene glycol)," *Carbon*, vol. 45, no. 5, pp. 1051–1057, 2007.

[32] C. K. Najeeb, J.-H. Lee, J.-H. Kim, and D. Kim, "Highly efficient individual dispersion of single-walled carbon nanotubes using biocompatible dispersant," *Colloids and Surfaces B: Biointerfaces.*, vol. 102, pp. 95–101, 2013.

[33] O. V. Kharissova, B. I. Kharisov, and E. G. de Casas Ortiz, "Dispersion of carbon nanotubes in water and non-aqueous solvents," *RSC Advances*, vol. 3, no. 47, 2013.

[34] B. I. Kharisov, O. V. Kharissova, and A. V. Dimas, "The dispersion, solubilization and stabilization in "Solution" of single-walled carbon nanotubes," *RSC Advances*, vol. 6, no. 73, pp. 68760–68787, 2016.

[35] B. Zhang and T. Chen, "Study of ultrasonic dispersion of graphene nanoplatelets," *Materials*, vol. 12, no. 11, p. 1757, 2019.

[36] V. Shabafrooz, S. Bandla, and J. C. Hanan, "Graphene/poly(ethylene glycol) dispersions for fabrication of nanocomposites: effects of dispersion processing conditions," *Graphene Technology*, vol. 3, no. 2-4, pp. 47–56, 2018.

[37] F. Zhao, L. Ling, L. Liu, A. Zafar, and Z. Ni, "The dispersion of graphene in conductive epoxy composites investigated by Raman spectroscopy," *Journal of Raman Spectroscopy*, vol. 48, no. 3, pp. 432–436, 2017.

[38] H. Gao, G. Hu, and H. Liu, "Preparation of a highly stable dispersion of graphene in water with the aid of graphene oxide," *Industrial & Engineering Chemistry Research*, vol. 58, no. 38, pp. 17842–17849, 2019.

[39] Z. S. Metaxa and S. K. Kourkoulis, "Dispersion of graphene nanoplatelets reinforcing type II cement paste," *Procedia Structural Integrity*, vol. 13, pp. 2011–2016, 2018.

[40] A. F. Ghanem and M. H. Abdel Rehim, "Assisted tip sonication approach for graphene synthesis in aqueous dispersion," *Biomedicines*, vol. 6, no. 2, p. 63, 2018.

[41] M. Ma, J. Song, L. Bai et al., "Effect of H-bonding effect on reverse micelle extraction of bovine serum albumin," *Journal of Dispersion Science and Technology*, pp. 1–7, 2019.

[42] H. Ghodrati and R. Ghomashchi, "Effect of graphene dispersion and interfacial bonding on the mechanical properties of metal matrix composites: an overview," *FlatChem*, vol. 16, p. 100113, 2019.

[43] G. Ciofani, V. Raffa, V. Pensabene, A. Menciassi, and P. Dario, "Dispersion of multi-walled carbon nanotubes in aqueous Pluronic F127 solutions for biological applications," *Fullerenes, Nanotubes, and Carbon Nanostructures*, vol. 17, no. 1, pp. 11–25, 2009.

[44] N. R. Arutyunyan and D. V. Baklashev, "Obraztsova EDJ-TEPJB. Suspensions of single-wall carbon nanotubes stabilized by pluronic forbiomedical applications," *The European Physical Journal B*, vol. 75, no. 2, pp. 163–166, 2010.

[45] V. C. Moore, M. S. Strano, E. H. Haroz et al., "Individually suspended single-walled carbon nanotubes in various surfactants," *Nano Letters*, vol. 3, no. 10, pp. 1379–1382, 2003.

[46] J. Pang, G. Xu, Y. Tan, and F. He, "Water-dispersible carbon nanotubes from a mixture of an ethoxy-modified trisiloxane and pluronic block copolymer F127," *Colloid and Polymer Science*, vol. 288, no. 18, pp. 1665–1675, 2010.

[47] X. Xin, G. Xu, T. Zhao et al., "Dispersing carbon nanotubes in aqueous solutions by a starlike block copolymer," *The Journal of Physical Chemistry C*, vol. 112, no. 42, pp. 16377–16384, 2008.

[48] Y. Yan, L. Piao, S.-H. Kim, W. Li, and H. Zhou, "Effect of Pluronic block copolymers on aqueous dispersions of graphene oxide," *RSC Advances*, vol. 5, no. 50, pp. 40199–40204, 2015.

[49] S. Parveen, S. Rana, R. Fangueiro, and M. C. Paiva, "Characterizing dispersion and long term stability of concentrated carbon nanotube aqueous suspensions for fabricating ductile cementitious composites," *Powder Technology*, vol. 307, pp. 1–9, 2017.

[50] S. Parveen, S. Rana, R. Fangueiro, and M. C. Paiva, "Microstructure and mechanical properties of carbon nanotube reinforced cementitious composites developed using a novel dispersion technique," *Cement and Concrete Research*, vol. 73, pp. 215–227, 2015.

[51] S. Shamsi, F. M. Yasin, S. N. E. Sarchio, and D. Perumal, "Characterization of nano-graphene oxide stabilized by Pluronic as a nanocarrier," *Frontiers in Pharmacology*, vol. 9, 2018.

[52] M. F. Islam, E. Rojas, D. M. Bergey, A. T. Johnson, and A. G. Yodh, "High weight fraction surfactant solubilization of single-wall carbon nanotubes in water," *Nano Letters*, vol. 3, no. 2, pp. 269–273, 2003.

[53] L. Lin, H. Peng, and G. Ding, "Dispersion stability of multi-walled carbon nanotubes in refrigerant with addition of surfactant," *Applied Thermal Engineering*, vol. 91, pp. 163–171, 2015.

[54] J. Wang, J. Sun, L. Gao et al., "Improving the conductivity of single-walled carbon nanotubes films by heat treatment," *Journal of Alloys and Compounds*, vol. 485, no. 1-2, pp. 456–461, 2009.

[55] W. S. Sarsam, A. Amiri, S. N. Kazi, and A. Badarudin, "Stability and thermophysical properties of non-covalently functionalized graphene nanoplatelets nanofluids," *Energy Conversion and Management.*, vol. 116, pp. 101–111, 2016.

[56] R. M. F. Fernandes, B. Abreu, B. Claro et al., "Dispersing carbon nanotubes with ionic surfactants under controlled conditions: comparisons and insight," *Langmuir*, vol. 31, no. 40, pp. 10955–10965, 2015.

[57] "Carbon nanotube characterization, MWCNT/ Part Number: GCM327 101 N Commerce St., Madisonville, Texas, 77864, United States/ Phone: (936) 207-9334," Cnplus, 2019, January 2019, https://cnplus.us/inc/sdetail/168.

[58] "Graphene nanoplatelets characterization, GNP/ Part Number: TGN201 101 N Commerce St., Madisonville, Texas, 77864, United States/ Phone: (936) 207-9334," Cnplus, 2019, January 2019, https://cnplus.us/inc/sdetail/269.

[59] I. Madni, C.-Y. Hwang, S.-D. Park, Y.-H. Choa, and H.-T. Kim, "Mixed surfactant system for stable suspension of multiwalled carbon nanotubes," *Colloids and Surfaces A: Physicochemical and Engineering Aspects*, vol. 358, no. 1-3, pp. 101–107, 2010.

[60] https://www.sigmaaldrich.com/catalog/product/aldrich/289957?lang=pt&region=PT.

[61] https://www.standard-sand.com/en/standard-sand-bs-4550/.

[62] J. Yu, N. Grossiord, C. E. Koning, and J. Loos, "Controlling the dispersion of multi-wall carbon nanotubes in aqueous surfactant solution," *Carbon*, vol. 45, no. 3, pp. 618–623, 2007.

[63] J. S. Lauret, C. Voisin, G. Cassabois et al., "Ultrafast carrier dynamics in single-wall carbon nanotubes," *Physical Review Letters*, vol. 90, no. 5, article 057404, 2003.

[64] B. White, S. Banerjee, S. O'Brien, N. J. Turro, and I. P. Herman, "Zeta-potential measurements of surfactant-wrapped individual single-walled carbon nanotubes," *The Journal of Physical Chemistry C*, vol. 111, no. 37, pp. 13684–13690, 2007.

[65] J. Lee, M. Kim, C. K. Hong, and S. E. Shim, "Measurement of the dispersion stability of pristine and surface-modified multiwalled carbon nanotubes in various nonpolar and polar solvents," *Measurement Science and Technology*, vol. 18, no. 12, pp. 3707–3712, 2007.

[66] R. H. Kretsinger, V. N. Uversky, and E. A. Permyakov, Eds., "UV-vis, ultraviolet-visible spectroscopy," in *Encyclopedia of Metalloproteins*, p. 2292, New York, NY: Springer New York, 2013.

[67] H. Yu, S. Hermann, S. E. Schulz, T. Gessner, Z. Dong, and W. J. Li, "Optimizing sonication parameters for dispersion of single-walled carbon nanotubes," *Chemical Physics*, vol. 408, pp. 11–16, 2012.

[68] Z. Baig, O. Mamat, M. Mustapha, A. Mumtaz, K. S. Munir, and M. Sarfraz, "Investigation of tip sonication effects on structural quality of graphene nanoplatelets (GNPs) for superior solvent dispersion," *Ultrasonics Sonochemistry*, vol. 45, pp. 133–149, 2018.

[69] M. S. Strano, V. C. Moore, M. K. Miller et al., "The role of surfactant adsorption during ultrasonication in the dispersion of single-walled carbon nanotubes," *Journal of Nanoscience and Nanotechnology.*, vol. 3, no. 1, pp. 81–86, 2003.

[70] W. Chen, L. Yan, and P. R. Bangal, "Preparation of graphene by the rapid and mild thermal reduction of graphene oxide induced by microwaves," *Carbon*, vol. 48, no. 4, pp. 1146–1152, 2010.

[71] S. M. Goodman, N. Ferguson, and A. B. Dichiara, "Lignin-assisted double acoustic irradiation for concentrated aqueous dispersions of carbon nanotubes," *RSC Advances*, vol. 7, no. 9, pp. 5488–5496, 2017.

[72] J. G. Speight, "A review of: "Surfactants and interfacial phenomena"," *Energy Sources*, vol. 27, no. 8, p. 779, 2006.

[73] L. Vaisman, H. D. Wagner, and G. Marom, "The role of surfactants in dispersion of carbon nanotubes," *Advances in Colloid and Interface Science*, vol. 128-130, pp. 37–46, 2006.

[74] J. N. Coleman, "Liquid-phase exfoliation of nanotubes and graphene," *Advanced Functional Materials*, vol. 19, no. 23, pp. 3680–3695, 2009.

[75] Z. Sun, V. Nicolosi, D. Rickard, S. D. Bergin, D. Aherne, and J. N. Coleman, "Quantitative evaluation of surfactant-stabilized single-walled carbon nanotubes: dispersion quality and its correlation with zeta potential," *The Journal of Physical Chemistry C.*, vol. 112, no. 29, pp. 10692–10699, 2008.

[76] N. Grossiord, P. J. J. Kivit, J. Loos et al., "On the influence of the processing conditions on the performance of electrically conductive carbon nanotube/polymer nanocomposites," *Polymer*, vol. 49, no. 12, pp. 2866–2872, 2008.

[77] V. Sa and K. G. Kornev, "Analysis of stability of nanotube dispersions using surface tension isotherms," *Langmuir*, vol. 27, no. 22, pp. 13451–13460, 2011.

[78] S. Utsumi, M. Kanamaru, H. Honda et al., "RBM band shift-evidenced dispersion mechanism of single-wall carbon nanotube bundles with NaDDBS," *Journal of Colloid and Interface Science*, vol. 308, no. 1, pp. 276–284, 2007.

[79] R. J. Smith, M. Lotya, and J. N. Coleman, "The importance of repulsive potential barriers for the dispersion of graphene using surfactants," *New Journal of Physics*, vol. 12, no. 12, p. 125008, 2010.

[80] W. Wenseleers, I. I. Vlasov, E. Goovaerts, E. D. Obraztsova, A. S. Lobach, and A. Bouwen, "Efficient isolation and solubilization of pristine single-walled nanotubes in bile salt micelles," *Advanced Functional Materials*, vol. 14, no. 11, pp. 1105–1112, 2004.

[81] B. Sohrabi, N. Poorgholami-Bejarpasi, and N. Nayeri, "Dispersion of carbon nanotubes using mixed surfactants: experimental and molecular dynamics simulation studies," *The Journal of Physical Chemistry B*, vol. 118, no. 11, pp. 3094–3103, 2014.

[82] B. Vigolo, A. Pénicaud, C. Coulon et al., "Macroscopic fibers and ribbons of oriented carbon nanotubes," *Science*, vol. 290, no. 5495, pp. 1331–1334, 2000.

[83] "March's Advanced Organic Chemistry: Reactions,Mechanisms, and Structure. Sixth EditionBy Michael B. Smith and Jerry March. John Wiley & Sons, Inc., Hoboken, NJ. 2007. xx + 2354 pp. 16 × 24 cm. ISBN 978-0-471-72091-1. $99.95," *Journal of Medicinal Chemistry*, vol. 50, no. 9, pp. 2279-2280, 2007.

[84] P. Stynoski, P. Mondal, and C. Marsh, "Effects of silica additives on fracture properties of carbon nanotube and carbon fiber reinforced Portland cement mortar," *Cement and Concrete Composites*, vol. 55, pp. 232–240, 2015.

[85] O. A. Mendoza Reales and R. Dias Toledo Filho, "A review on the chemical, mechanical and microstructural characterization of carbon nanotubes-cement based composites,"

Construction and Building Materials, vol. 154, no. 154, pp. 697–710, 2017.

[86] F. Hamidi and F. Aslani, "Additive manufacturing of cementitious composites: materials, methods, potentials, and challenges," *Construction and Building Materials.*, vol. 218, pp. 582–609, 2019.

[87] S. Alrekabi, A. B. Cundy, A. Lampropoulos, R. L. D. Whitby, and I. Savina, "Mechanical performance of novel cement-based composites prepared with nano-fibres, and hybrid nano- and micro-fibres," *Composite Structures*, vol. 178, pp. 145–156, 2017.

[88] A. Naqi, N. Abbas, N. Zahra, A. Hussain, and S. Q. Shabbir, "Effect of multi-walled carbon nanotubes (MWCNTs) on the strength development of cementitious materials," *Journal of Materials Research and Technology*, vol. 8, no. 1, pp. 1203–1211, 2019.

[89] K. Yamada, T. Takahashi, S. Hanehara, and M. Matsuhisa, "Effects of the chemical structure on the properties of polycarboxylate-type superplasticizer," *Cement and Concrete Research*, vol. 30, no. 2, pp. 197–207, 2000.

[90] G. Jing, Z. Ye, X. Lu, and P. Hou, "Effect of graphene nanoplatelets on hydration behaviour of Portland cement by thermal analysis," *Advances in Cement Research*, vol. 29, no. 2, pp. 63–70, 2017.

[91] S. Sharma and N. C. Kothiyal, "Facile growth of carbon nanotubes coated with carbon nanoparticles: a potential low-cost hybrid nanoadditive for improved mechanical, electrical, microstructural and crystalline properties of cement mortar matrix," *Construction and Building Materials.*, vol. 123, pp. 829–846, 2016.

[92] E. Knapen and D. Van Gemert, "Cement hydration and microstructure formation in the presence of water-soluble polymers," *Cement and Concrete Research.*, vol. 39, no. 1, pp. 6–13, 2009.

[93] F. Ridi, E. Fratini, F. Mannelli, and P. Baglioni, "Hydration process of cement in the presence of a cellulosic additive. A calorimetric investigation," *The Journal of Physical Chemistry B.*, vol. 109, no. 30, pp. 14727–14734, 2005.

[94] M. S. Konsta-Gdoutos, Z. S. Metaxa, and S. P. Shah, "Highly dispersed carbon nanotube reinforced cement based materials," *Cement and Concrete Research*, vol. 40, no. 7, pp. 1052–1059, 2010.

[95] M. S. Konsta-Gdoutos, Z. S. Metaxa, and S. P. Shah, "Multi-scale mechanical and fracture characteristics and early-age strain capacity of high performance carbon nanotube/cement nanocomposites," *Cement and Concrete Composites*, vol. 32, no. 2, pp. 110–115, 2010.

[96] W. Dong, W. Li, Z. Tao, and K. Wang, "Piezoresistive properties of cement-based sensors: review and perspective," *Construction and Building Materials.*, vol. 203, pp. 146–163, 2019.

[97] B. Han, S. Ding, and X. Yu, "Intrinsic self-sensing concrete and structures: a review," *Measurement*, vol. 59, pp. 110–128, 2015.

[98] S. Berber, Y.-K. Kwon, and D. Tománek, "Unusually high thermal conductivity of carbon nanotubes," *Physical Review Letters*, vol. 84, no. 20, pp. 4613–4616, 2000.

[99] C. Liu, G. Liu, Z. Ge, Y. Guan, Z. Cui, and J. Zhou, "Mechanical and Self-Sensing Properties of Multiwalled Carbon Nanotube- Reinforced ECCs," *Advances in Materials Science and Engineering*, vol. 2019, 9 pages, 2019.

[100] A. O. Monteiro, P. B. Cachim, and P. M. F. J. Costa, "Self-sensing piezoresistive cement composite loaded with carbon black particles," *Cement and Concrete Composites*, vol. 81, pp. 59–65, 2017.

[101] J. Donnini, T. Bellezze, and V. Corinaldesi, "Mechanical, electrical and self-sensing properties of cementitious mortars containing short carbon fibers," *Journal of Building Engineering*, vol. 20, pp. 8–14, 2018.